Organic & Biomolecular Chemistry

ROYAL SOCIETY OF CHEMISTRY

PAPER

View Article Online
View Journal | View Issue

Cite this: *Org. Biomol. Chem.*, 2025, **23**, 9142

Thiosquaramides: dual-function ionophores for Zn^{2+} and Cl^- with ion dependent anti-microbial activity

Xuanyang Luo, [a] Luke E. Brennan,[a,b] Chris S. Hawes, [c] Tobias Krämer, [a] John Farragher,[b] Shane Robinson,[b,d] Kevin Kavanagh[b,e] and Robert B. P. Elmes *[a,b,f]

Synthetic transmembrane transporters have garnered considerable interest in medicinal chemistry for their ability to modulate cellular processes *via* ion transport. These ionophores can disrupt intracellular ion homeostasis, often triggering biological responses such as programmed cell death or antimicrobial effects. In this study, we present a series of thionated squaramides that demonstrate dual binding affinity for both metal cations and anionic species, as confirmed by spectroscopic analyses and single-crystal X-ray crystallography. While thiosquaramides have previously been shown to mediate chloride transport across lipid bilayers, we now report their capacity to facilitate Zn^{2+} transport, as assessed using the FluoZin-3 fluorescence assay in a vesicle model. Notably, the ability of these thiosquaramides to act as zinc ionophores correlates with a distinct Zn^{2+}-dependent antimicrobial response against *Staphylococcus aureus*. These findings establish a clear link between zinc transport and biological activity, suggesting that thiosquaramides function through a novel ionophoric mode of action. Collectively, this work introduces a new class of dual-function ionophores with potential as antimicrobial agents and underscores the value of structural diversification in the design of supramolecular therapeutics.

Received 18th July 2025,
Accepted 19th September 2025

DOI: 10.1039/d5ob01166c

rsc.li/obc

Introduction

Squaramides have seen an explosion of research interest in recent years due to several favourable characteristics that provide applicability across diverse sections of the chemical and biological sciences.[1–3] This applicability has included organocatalysis, bioconjugation and sensors to name just a few key areas.[4–6] To a large extent, squaramides have also been exploited in the field of anion recognition, sensing and transport[7–20] where their ability to act as anionophores has seen them applied as potential anti-cancer and anti-microbial therapeutics.[21,22] However, while the number of examples of oxosquaramide derivatives continues to increase, examples of their thionated derivatves, thiosquaramides have remained more scarce.[23,24] McGouran and co-workers have synthesised a range of nucleoside derivatives modified with thiosquaramide where they have shown their ability to act as inhibitors of SNM1A; a zinc-dependent nuclease involved in the removal of interstrand crosslink lesions from DNA.[24] Jolliffe and co-workers have reported a series of thiosquaramides that display switchable anion recognition and transport, where reversible anion transport was demonstrated by simply modulating pH.[23,25] While it has been suggested that, squaramides should also be capable of cation recognition, this is a characteristic that remains largely unexplored.[16,24,26] One of our main interests in this area, is the synthesis of squaramide based receptors that are also capable of efficient ionophoric activity and their potential use in medicinal chemistry.[26–29] Most recently, we have demonstrated efficient anti-microbial activity against Gram-positive bacteria such as *Staphylococcus aureus* and Methicillin Resistant *Staphylococcus aureus* (MRSA), where the activity was linked to the ability of the receptors to efficiently disrupt chloride homestasis.[30,31] While this approach has yielded some interesting new approaches to antimicrobial development, there remains significant potential to expand the scope through targeting other ions – particularly cationic species. Indeed, many well known antibiotics such as valinomycin and monensin are known to exert their anti-microbial effects through ionophorism of Na^+ and K^+ ions.[32–34] Similarly, Zn^{2+} ionophorism is emerging

[a]*Department of Chemistry, Maynooth University, National University of Ireland, Maynooth, Co. Kildare, Ireland. E-mail: robert.elmes@mu.ie*
[b]*SSPC – the Science Foundation Ireland Research Centre for Pharmaceuticals, University of Limerick, V94 T9PX Limerick, Ireland*
[c]*School of Chemical and Physical Sciences, Keele University, Keele, ST5 5BG, UK*
[d]*Janssen Pharmaceutical Sciences, Cork, T45 P663, Ireland*
[e]*Department of Biology, Maynooth University, National University of Ireland, Maynooth, Co. Kildare, Ireland*
[f]*Kathleen Lonsdale Institute for Human Health Research, Maynooth University, National University of Ireland, Co. KildareW23 F2H6 Maynooth, Ireland*

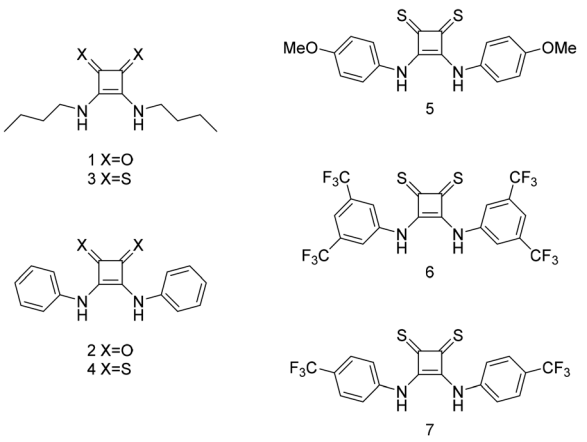

Fig. 1 The chemical structures of the squaramide receptors under study.

as a promising modality for new antimicrobial agents.[35] For example, known zinc ionophore PBT2, in combination with Zn^{2+}, has been shown to reverse Gram-positive bacterial resistance against several antibiotics.[36] The same ionophore mediates activity against *Streptococcus uberis*, by the accumulation of Zn^{2+} and the depletion of Mn^{2+} that triggers an increase in oxidative stress.[37] Such a supramolecular approach to antimicrobial development is an emerging field,[38] but there is clearly a need for more structural diversity amongst the ionophore families that will lead to new antimicrobial drugs that exert their activity through novel modes of action – an important need during the current crisis in antimicrobial resistance. With this in mind, we have synthesised a series of oxo- and thiosquaramides (**1–7**, Fig. 1) and explored their ability to bind either anions or cations using NMR and UV-vis spectroscopies. We have found that metal binding to oxosquaramides appears to be weak under competitive solvent conditions but is significantly increased with their thio analogues which show clear evidence of binding to 2^+ metals (such as Zn^{2+}, Cd^{2+}, Pb^{2+} and Hg^{2+}). The binding event is easily observed using UV/vis spectroscopy and appears to occur in a 2 : 1 (ligand : metal) stoichiometry in certain solvents. Moreover, as part of this work, we confirm for the first time, that thiosquaramides are also capable of rapid and efficient Zn^{2+} transport, acting as potent zinc ionophores in a liposome model with comparable efficiency to the known clinically available Zn^{2+} ionophore, clioquinol. Moreover, we also show that thiosquaramides are capable of dose dependent antimicrobial activity in *Staphylococcus aureus* that is enhanced in the presence of Zn^{2+}, suggesting that ionophoric activity may be related to the observed anti-microbial effect.

Results and discussion

Synthesis and characterisation

Oxosquaramides **1** and **2** were synthesized using diethyl squarate and the appropriate primary amine in the presence of Zn $(OTf)_2$ as previously reported.[39] Thiosquaramides **3–7** were obtained using dicyclopentyl thiosquarate as the key intermediate through reaction with the appropriate primary amine in MeCN.[40,41] This method allowed the formation of thiosquaramides **3–7** in 31%, 71%, 62%, 42%, 56% yields, respectively. All compounds were fully characterised using ^{1}H and ^{13}C NMR, HRMS, IR and LCMS (see the SI for full characterisation details) and where literature compounds were made, all data matched the literature.

Thiosquaramide **3** was crystallised from hot MeCN, and analysis by single crystal X-ray diffraction confirmed the expected structure. Compound **3** forms a one-dimensional hydrogen bonded chain in the solid state as shown in Fig. 2(a), comprised of $R_2^2(10)$ rings between the N–H donors and sulfur acceptors at D···A distances of 3.4188(6) Å. Although the interactions are directional, the peripheral butyl chains provide no significant inter-chain interactions with the result that there is no transfer of directionality from one chain to the next, and the overall structure is a disordered average of chains proceeding both in the positive and negative *b* directions. ^{1}H NMR variable concentration experiments support the occurrence of similar interactions in solution where significant downfield shifts of the NH signals for compound **3** are observed as a function of increasing concentration, suggesting that some aggregation behaviour also occurs in MeCN solution (Fig. S29).

One interesting observation also warrants comment. When a sample of **3** was exposed to water for a period of several weeks, a trace quantity of a second crystalline phase was isolated. The structural model, refined in the trigonal space group $R\bar{3}$, revealed compound **3** alongside butylammonium cations and sulfate anions, presumably arising from gradual hydrolysis and oxidation of **3**. The overall structure takes the form of a linear assembly of three sulfate anions, capped at each end by three molecules of **3** with an equatorial belt of six butylammonium cations, as shown in Fig. 2(b) and S84. The central sulfate and the inner face of the terminal sulfates are supported by hydrogen bonds from the butylammonium cations, while the thiosquaramides form a 3-fold propeller with chelating $R_2^2(9)$ hydrogen bonding interactions to the terminal sulfate groups. This motif is reminiscent of that seen in tripodal urea-based anion receptors such as the sulfate receptor reported by Das[42] although the shorter N···O distance in the case of **3** (2.765(3) and 2.864(3) Å, *cf.* 2.87–2.90 Å in the urea case) may indicate a greater N–H acidity for the thiosquaramide. While indicating that thiosquaramides may suffer from long term stability problems in the presence of aqueous solutions, this observation can also be seen as further evidence of their strong anion-binding capabilities, particularly toward polyvalent anions such as sulfate, and highlights the potential for these systems to form discrete supramolecular assemblies under conditions of slow crystallization or degradation.

Photophysical evaluation

Given the distinct chromophoric nature of squaramides and thiosquaramides, we wished to conduct a preliminary analysis of the UV/Vis absorption properties of receptors **1–7**. We antici-

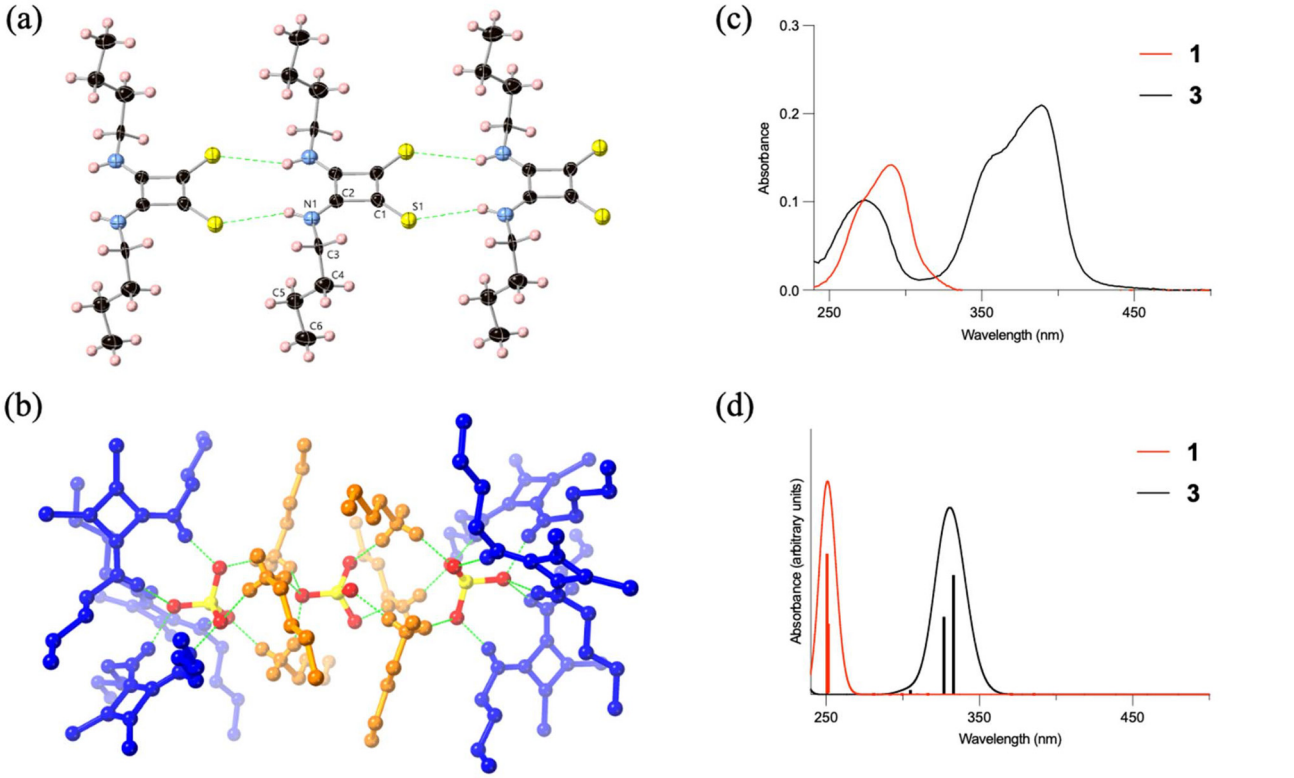

Fig. 2 (a) Crystal structure of **3** with labels for unique heteroatoms. Disorder is omitted for clarity. (b) Complete structure of $(BuNH_3)6(\mathbf{3})6(SO_4)_3$ with thiosquaramide molecules coloured blue and butylammonium species coloured orange, selected hydrogen atoms and disorder in the central sulfate are omitted for clarity. UV spectrum of receptors **1** and **3** in MeCN solution. (c) Experimental and (d) computational UV spectrum of receptors **1** and **3** in MeCN solution.

pated a significant difference in their properties and suspected that this information may be useful when attempting to determine ion binding behaviour. An absorption band at 291 nm was observed for **1** in MeCN while for the thiosquaramide analogue **3**, two bands are observed with λ_{max} of 274 nm and 388 nm, respectively (Fig. 2(c) and (d)). Similar behaviour was observed for receptor **2** which exhibited λ_{max} of 328 nm while **4** showed absorption maxima at 288 nm and 408 nm. In MeCN, a significant difference between the oxo- and thio-derivatives was observed where inclusion of the sulfur atoms appears to result in a significant red shift of the absorption. We expected that compared to C═O, the weaker bond strength of C═S reduces the energy of electronic transitions which results in the red shift of λ_{max}.[43] This trend was observed for all analogues. Moreover, solutions of oxo-squaramides **1** and **2** appeared colourless, while solutions of all thio-derivatives appeared yellow/orange. Insight into the spectral differences of the oxo- *vs.* thiosquaramides were obtained from time-dependent density functional theory (TD-DFT) calculations performed on models of receptors **1–4**. The calculated absorption spectra (Fig. S75 and S76) are consistent with the spectral features of the experimental data and accurately reproduce the red shift of the absorption bands for the thio congeners. The spectrum of **1** shows one peak centred around 251 nm with dominant contributions from two nearly coalescing HOMO → LUMO (250.7 nm) and HOMO → LUMO+1 (251.5 nm) transitions (Fig. S77). These peaks are more separated in **3**, splitting into transitions that appear at 333 and 327 nm, respectively. A smaller shoulder around 305 nm in the computed spectrum corresponds to a HOMO−1 → LUMO+1 transition which is best described having n → π* character (Fig. S78). This is consistent with the general observation that this absorption band is shifted into the visible spectral region for thiocarbonyl compounds as compared to the corresponding carbonyl derivatives. Similar behaviour is seen for the pair **2** and **4**, with additional peaks emerging at 230 and 250 nm in these cases, respectively, due to transitions from the C═S π-orbital into the LUMO (Fig. S78 and S80). The red shift of the absorptions in **2** and **4** can be attributed to the energy lowering of the LUMO and LUMO+1 in these thiocarbonyl derivatives, leading to an overall narrowing of the energy gap in the frontier orbital region (Fig. S81 and S82). Considering the longer C═S bond lengths and the differences in 2p and 3p orbital size, this effect can be understood in terms of the weaker overlap between the C(2p) and S(3p) orbitals compared to carbonyl valence C(2p)/O(2p) interactions.[44] This effect can also be correlated to the lower relative bond strengths of the thiocarbonyl *versus* carbonyl unit, as reflected in their respective stretching force constants (Table S3).

Ion binding studies

Given the observed absorption characteristics of these receptors we expected that complexation to either anionic or cationic species may result in a perturbation of their ground state properties. Squaramides are well known in the literature for their H-bond donating ability as well as their H-bond accepting ability. This has meant they are often reported as efficient anion binders. However, their properties as cation binding receptors are much less well developed. There are very few examples of this, and as far as we are aware, there have not been any reports of metal binding studies with thiosquaramides. We first carried out anion binding titrations to observe any significant difference in behaviours between the oxo- *vs.* thio-analogues. Fabbrizzi and co-workers have previously examined the binding behaviour of a nitro-squaramide analogue using UV/Vis spectrophotometric titration experiments where they showed interaction of Cl^- at the squaramide NHs induces a red shift in the absorption spectrum due to stabilisation of one or more excited states.[45] Thus, we expected similar behaviour might be observed in this case. To evaluate the anion binding properties of receptors **1–4**, we conducted titrations with tetrabutylammonium chloride (TBACl) in MeCN and monitored the changes using UV-Vis spectroscopy. All receptors exhibited a red shift in their absorption maxima upon Cl^- addition, indicative of Cl^- binding at the squaramide/thiosquaramide moieties. As representative examples, the titrations of oxosquaramide **2** and thiosquaramide **4** with Cl^- showed bathochromic shifts of several nm in both cases (Fig. 3a and b). These spectral changes were analysed using the open-access BindFit software, with the data for most receptors fitting best to a 2 : 1 host : guest binding model (see Fig. S22–S28) and showing a higher affinity of the thiosquaramide derivatives in comparison to their oxosquaramide analogues.[46,47]

To complement the UV-Vis data and further confirm the binding, ^{1}H NMR titrations of receptors **1–4** were also carried out in either CD_3CN or DMSO-d_6 (depending on solubility) at 298 K, again using TBACl as the Cl^- source. The changes in chemical shifts ($\Delta\delta$) were plotted against equivalents of Cl^- and again fitted using BindFit. These studies also generally supported a 2 : 1 binding stoichiometry in CD_3CN while titrations carried out in DMSO-d_6, were best fitted to a 1 : 1 model. For example, the ^{1}H NMR titration of thiosquaramide **4** with Cl^- in DMSO-d_6 (Fig. 3(e)) showed substantial downfield shifts of the squaramide NH signals, consistent with anion binding and was best fitted to a 1 : 1 model as previously reported.[23] However, when the titration was repeated in a CD_3CN/DMSO-d_6 (49 : 1) mixture Job's plot analysis supported a 2 : 1 model (Fig. S35). Such an observation suggests that the choice of solvent has a strong influence on the Cl^- binding affinity and stoichiometry with these receptors.

To assess metal binding capacity of receptors **1–4**, cation binding studies were also conducted using UV-Vis spectroscopy. A metal screening experiment was performed by adding 1 equiv. of various metal perchlorate salts (Fe^{3+}, Hg^{2+}, Pb^{2+}, Cd^{2+}, Zn^{2+}, K^+, Li^+, Ca^{2+}, Na^+, Ni^{2+}, Cu^{2+}, Co^{2+}) to a solution of the receptor (10 μM) in MeCN. The most significant spectral changes were observed for thiosquaramides **3** and **4** upon addition of Cd^{2+}, Pb^{2+}, Hg^{2+}, and Zn^{2+}, prompting further detailed titration studies with these metals (Fig. S36). UV-Vis titrations with these metal cations showed a clear contrast between oxosquaramides and thiosquaramides: the former showing very minor spectral changes, while the latter exhibiting dramatic shifts upon metal addition. For instance, addition of 10 equiv. Zn^{2+} to receptor **2** caused minimal changes, whereas just 3.5 equiv. Zn^{2+} added to receptor **4** resulted in significant hypochromism at 404 nm, a red shift to 410 nm, and pronounced changes at 290 nm and 330 nm, along with the appearance of isosbestic points at 305 nm and 335 nm (Fig. 3c and d). These changes were accompanied by visible color changes, indicating strong metal–receptor interaction (see Fig. S57). Similar behaviour was also observed for Cd^{2+} and Pb^{2+}. To assess the effect of substituents on metal binding, we extended these titrations to receptors and **5–7** showing that all thiosquaramide derivatives displayed high sensitivity toward Cd^{2+}, Pb^{2+}, Hg^{2+}, and Zn^{2+}, with similar spectral profiles and shifts. The resulting titration data were fitted using BindFit, yielding association constants (K_a) in the range of 10^5–10^6 M^{-1}, typically best described again by a 2 : 1 receptor : metal binding model. Notably, a Job's plot analysis of receptor **3** with Zn^{2+} confirmed a 2 : 1 stoichiometry in MeCN (see Fig. S35), consistent with the BindFit results and reinforcing the conclusion that higher-order complexation appears to occur under the studied conditions.

Crystal structure analysis also supported the ability of thiosquaramides to form a 2 : 1 complex with 2+ metal salts. The reaction of compound **4** with lead(II) perchlorate in MeCN gave small yellow plate crystals, analysis of which by X-ray diffraction revealed a complex of the form $[Pb(\mathbf{4})_2]2ClO_4$ as shown in Fig. 3(f) and Fig. S85 with the asymmetric unit containing two nearly equivalent residues. The Pb^{2+} ions adopt four coordinate distorted sawhorse geometries, where the thiosquaramides adopt asymmetric chelating coordination modes occupying the equatorial positions at much shorter distances than the axial positions (2.782(3)–2.825(3) Å for equatorial, *vs.* 2.915(3)–3.025(3) Å for the axial positions). The thiosquaramide C=S bonds are not significantly lengthened by coordination compared to those in the hydrogen-bonded sulfate adduct (*ca.* 1.65 Å). The extended structure of $[Pb(\mathbf{4})_2]2ClO_4$ reveals further association of $[Pb(\mathbf{4})_2]$ dications into discrete tetranuclear assemblies around two central perchlorate anions, with weaker Pb···O contacts involving the open faces of the lead ions mostly beyond 3 Å in length. As expected, the remaining perchlorate anions within the structure engage in hydrogen bonding with the thiosquaramide N–H groups, although from the enlarged ADPs these species appear to show more mobility or tendency for disorder than the perchlorate anions bound within the Pb_4 tetramer.

Ion transport studies

With the clear ability of thiosquaramides to bind to both anions and cations, we next wished to ascertain whether they

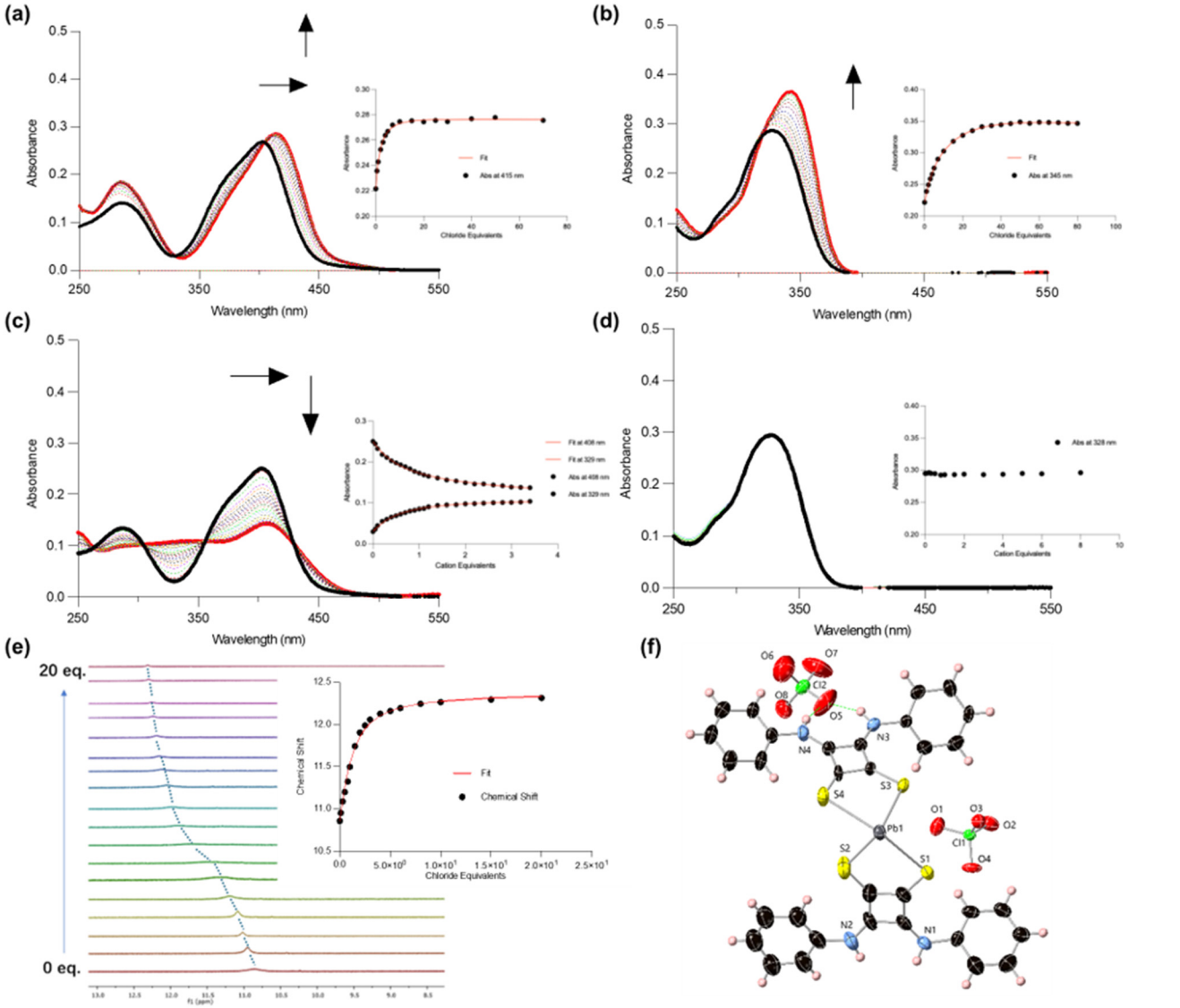

Fig. 3 (a) Absorption spectra of Cl^- titration of **4** in MeCN. (Inset) Fitplot for absorbance at 415 nm as a function of Cl^- concentration. The data was best fitted to a 2 : 1 binding model. (b) Absorption spectra of Cl^- titration of **2** in MeCN. (Inset) Fitplot for absorbance at 345 nm as a function of Cl^- concentration. The data was best fitted to a 2 : 1 binding model. (c) Zn^{2+} titration in MeCN with receptor **4**. (Inset) Fitplot for absorbance at 408 nm and 329 nm as a function of Zn^{2+} concentration. The data was best fitted to a 2 : 1 binding model. (d) Zn^{2+} titration in MeCN with receptor **2**. (Inset) Absorbance at 328 nm as a function of Zn^{2+} concentration. (e) ^1H NMR stackplot of **4** with TBACl in DMSO-d_6. (Inset): Fitplot for NH proton at δ = 10.86 ppm as function of Cl^- equivalents. The data was best fitted to a 1 : 1 binding model. (f) Representative structure of one of the two unique fragments in $[Pb(\mathbf{4})_2]2ClO_4$ with heteroatom labelling scheme. ADPs are rendered at the 50% probability level, hydrogen atoms and anion disorder are omitted for clarity.

might also be capable of ion transport. Squaramides and thiosquaramides are well-established as efficient chloride transporters,[23,25,48] and we have recently exploited this property in the development of antimicrobial agents.[30,31,49] We have also recently utilised the FluoZin-3 dye to confirm that hydroxychloroquine is not a direct zinc transporter[50] while also showing several other natural products are capable of efficient zinc transport.[51] Zinc transport is particularly, interesting from a biological perspective where it plays a significant role in many important biological processes. For example, Sensi and co-workers have recently shown that perturbation of zinc concentrations result in neurotoxic processes and affects neuronal functioning.[52] Moreover, Terao and co-workers have also shown that zinc ionophores, for example quercetin, result in antioxidant, anti-inflammatory, and neuroprotective effects in the central nervous system.[53,54] In this work, we again employed Large Unilamellar Liposomes (LUVs) to probe the ability of oxo- and thiosquaramides to act as ionophores.

To first probe metal ion transport, we again employed FluoZin-3-loaded Large Unilamellar Vesicles (LUVs), following our previously established methods[50,51] where LUVs composed of 1-palmitoyl-2-oleoyl-*sn-glycero*-3-phosphocholine (POPC)

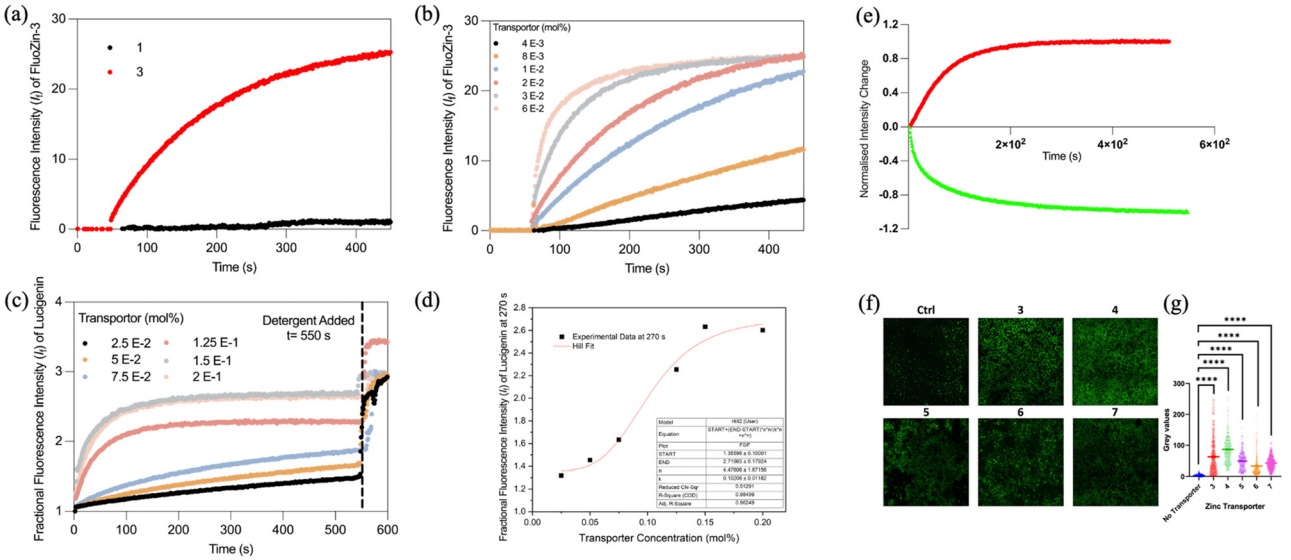

Fig. 4 (a) The change in fluorescence intensity over time of liposomes containing FluoZin-3 in PBS (0.01 M, pH = 7.4) upon the addition of Zn $(ClO_4)_2$ (0.1 mM) to receptors **1** (black, 5 μM) and **3** (red, 5 μM). (b) The dose-dependent change in fluorescence intensity of FluoZin-3 over time of liposomes containing FluoZin-3 in PBS (0.01 M, pH = 7.4) upon the addition of $Zn(ClO_4)_2$ (0.1 mM) followed by a pulse of **3** at a range of increasing concentrations. (c) The change of fractional fluorescent intensity with the addition of **3** and $ZnCl_2$ (75 μL, 0.5 M) to liposomes containing lucigenin (in 112.5 mM $Zn(NO_3)_2$) at various transporter concentrations (mol%). (d) Hill plot of the fractional fluorescence intensity with the addition of **3** and $ZnCl_2$ (75 μL, 0.5 M) to liposomes containing lucigenin (in 112.5 mM $Zn(NO_3)_2$) at various transporter concentrations (mol%) recorded at 270 s. (e) Normalised Zn^{2+} transport data of FluoZin-3 assays (red) *vs.* Cl^- transport data (green) of lucigenin assays of **3** (0.8 μM) under analogous conditions (225 mM $NaNO_3$). (f) Confocal laser scanning microscopy of unfixed POPC vesicles, comparing FluoZin-3 fluorescence before and after treatment with transporters **3**–**7**. (g) Analysis of the fluorescence intensity of FluoZin-3 across a 1000 μM ROI identified as the centre of each image, represented as mean grey values (+SEM) compared to control.

were prepared and loaded with FluoZin-3 in phosphate-buffered solution (PBS). Upon addition of $Zn(ClO_4)_2$ (0.1 mM) alone, no change in fluorescence was observed, confirming the dye was effectively encapsulated in the LUVs. However, subsequent addition of thiosquaramide derivatives (**3**–**7**) resulted in a rapid fluorescence increase, indicating Zn^{2+} transport into the vesicles. In contrast, oxosquaramide derivatives **1** and **2** showed no such activity, highlighting the importance of thionation for Zn^{2+} transport (Fig. 4a and S59). All five thiosquaramides displayed measurable ionophoric activity at 5 μM, with receptor **3** showing the highest transport rate. Interestingly, thiosquaramides bearing electron-withdrawing groups, known to enhance Cl^- transport, showed reduced Zn^{2+} transport, suggesting divergent structure–activity relationships for cation *vs.* anion transport. The Zn^{2+} transport activity of compound **3** was further quantified across different transporter : lipid ratios showing a classic dose dependent response (Fig. 4b). To our knowledge, this represents the first report of Zn^{2+} transport mediated by thiosquaramides.

We then turned to the question of whether metal ions can influence the known Cl^- transport activity of thiosquaramides. This time, lucigenin-loaded LUVs were used to assess Cl^- influx. To allow for direct comparison, $ZnCl_2$ was used across a range of transporter concentrations to determine EC_{50} values by Hill analysis and, as shown in Table 1, the EC_{50} for Cl^- transport by compound **3** in the presence of $ZnCl_2$ was ≈0.04 mol%, approximately threefold higher than that observed with NaCl (≈0.14 mol%) indicating that Zn^{2+} facilitates enhanced chloride transport.

Table 1 Summary of anion transport performance of **3** in $NaNO_3$ solution with different MCl pulse

Receptor	Ion	pH	EC_{50}[a]
3	$ZnCl_2$	7.2	0.04
	NaCl	7.2	0.14

[a] Concentration of receptors required to achieve the half of max effect.

To further explore the role of the metal salt, we conducted further lucigenin assays where the NO_3^- source in the LUV medium was replaced with $Zn(NO_3)_2$, $Cu(NO_3)_2$, $Cd(NO_3)_2$, Ni $(NO_3)_2$, or KNO_3, and Cl^- influx was then initiated with the corresponding MCl salt (Fig. 4c and Fig. S71–S79). The resulting EC_{50} values for compound **3** under these conditions (Table 2) revealed several trends: (1) K^+, Cu^{2+} and Na^+ produced similar EC_{50} values, suggesting minimal cation influence, (2) Ni^{2+} and Cd^{2+} significantly reduced Cl^- transport efficiency, suggesting a detrimental cation influence and (3) Zn^{2+} was again shown to increase Cl^- transport efficiency, suggesting a positive cation influence. Taken together, these results suggest that metals with strong binding affinities may hinder Cl^- transport through a weakening of anion binding. This is supported by ^1H NMR titration data, where the addition of Cl^- to a solution of receptor **3** in

Table 2 Summary of the EC_{50} value at 270 s for transporters **3** in different conditions

Metal ion	n^a	EC_{50}
Cu^{2+}	3.1	0.27
Zn^{2+}	4.5	0.10
Ni^{2+}	3.1	0.63
Na^+	2.7	0.13
K^+	2.5	0.25
Cd^{2+}	n.a[b]	n.a[b]

[a] Hill coefficient (*n*-value). [b] No observed transport behaviour.

the presence of Cd^{2+} caused almost no changes in the chemical shift of the NH protons, consistent with reduced propensity for anion binding (Fig. S34).

A spectrophotometric pK_a determination for receptor **3** also revealed a value of 5.9 (Fig. S21), indicating that deprotonation is also feasible under the conditions used, particularly with strong Lewis acids present, however, the solid-state structure does not show evidence of NH loss.

Despite these observations, Zn^{2+} uniquely enhances Cl^- transport, and suggests that a co-transport mechanism may be occurring with this metal, where Zn^{2+} and Cl^- are transported concurrently. Indeed, as shown in Fig. 4(e), time-dependent profiles from both FluoZin-3 and lucigenin assays, conducted under analogous conditions (225 mM $NaNO_3$), show closely matched kinetics, consistent with a coupled Zn^{2+}/Cl^- co-transport process mediated by thiosquaramide receptor **3**.

Finally, to further confirm the Zn^{2+} ionophoric ability of **3**, confocal microscopy was employed to observe the 'switch on' of FluoZin-3 fluorescence in POPC vesicles. POPC vesicles suspended in PBS (0.4 mM, in 0.01 M PBS) containing an excess of extravesicular Zn^{2+} ions were imaged before and after the addition of each receptor to a final concentration of 10 μM. Images were acquired using cumulative acquisition of 30% of each well stemming from the centre of a standard live-cell imaging compatible 96-well plate, with a Leica Stellaris 8 LSCM (WL laser 80% power, $\lambda_{exc/em}$ 494/516 nm, 10× non-immersion objective), and were stitched and deconvoluted using the in-house LasX software package. Fig. 4(f) and (g) show that, when compared to untreated vesicles, those treated with **3–7** for 5 min at 10 μM exhibit large increases in fluorescence intensity centred from the vesicles. Indeed, when Grey values (intensity) were measured for each image from the raw data, across a 1000 μm linear cross section of each image, and plotted relative to control, there is a clear, quantifiable increase in FluoZin-3 derived fluorescence when transporters are added to vesicles (up to 26-fold increase, $p < 0.0001$, multiple unpaired *t*-test) (Fig. 4g). This data provides additional qualitative visual evidence that supports the effective Zn^{2+} transport facilitated by receptor **3** already quantitatively measured by the FluoZin-3 assay.

Antimicrobial activity

Encouraged by the pronounced chloride transport activity observed in the presence of Zn^{2+}, we next sought to determine whether this enhanced transport translates into biological efficacy. As previously reported, we have developed a class of squaramide–indole hybrids ("squindoles") that display potent antimicrobial activity, mediated *via* anion transport mechanisms.[31] Given the well-established antimicrobial properties of known cation transporters such as Monensin, Valinomycin, Salinomycin, and Lasalocid,[55] we were motivated to investigate whether thiosquaramides **3–7** exhibit analogous behaviour through cation-associated pathways.

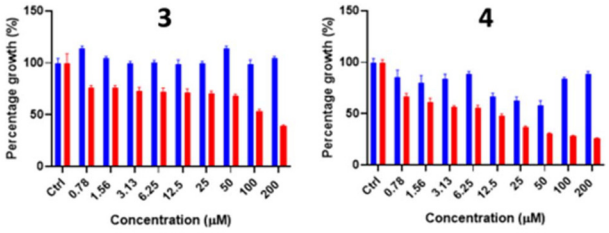

Fig. 5 Results of growth inhibition assays for **3** and **4** against *S. aureus*. Blue = transporter added in the absence of Zn^{2+}. Red = transporter added with 2 eq. excess of Zn^{2+}. Both results are represented as mean (+SEM) percentage growth relative to the control of three biological replicates.

To this end, we performed bacterial growth inhibition assays using *Staphylococcus aureus*. Cultures were grown to early stationary phase and incubated with each transporter across a range of concentrations, both in the absence and presence of Zn^{2+} (2 molar equivalents). Following a 24-hour incubation at 37 °C, bacterial growth was assessed *via* optical density measurements at 600 nm and normalised against untreated control samples.

The minimum inhibitory concentration required to inhibit 50% of bacterial growth (MIC_{50}) was derived for each compound from the resulting dose–response curves (see Fig. 5 and Fig. S83). The corresponding MIC_{50} values are summarised in Table 3. In each case, a marked enhancement in antimicrobial activity was observed when Zn^{2+} was co-administered. Notably, compound **4** exhibited an IC_{50} as low as 9.4 μM under zinc-rich conditions.

Although the enhancement was less dramatic for compounds **6** and **7**, an appreciable increase in activity was still evident, with MIC_{50} values improving to 32.5 μM and 25 μM respectively in the presence of Zn^{2+}. These findings support

Table 3 Summary of the MIC_{50} concentrations for transporters **3–7** against *S. aureus* in the absence and presence of 2 molar equivalents of Zn^{2+}

Receptor	MIC_{50} ($-Zn^{2+}$) (μM)	MIC_{50} ($+Zn^{2+}$) (μM)
3	n.a	100
4	n.a	9.4
5	n.a	25
6	50	33
7	50	25

n.a = no observed activity.

the hypothesis that Zn^{2+}-dependent ion transport plays a role in mediating the observed biological activity, and reinforce the potential of thiosquaramides as dual-function antimicrobial agents capable of modulating both cation and anion flux.

Conclusions

In conclusion, we have demonstrated that a series of thiosquaramides exhibit enhanced metal-binding affinity compared to their oxosquaramide analogues, with particular selectivity towards divalent metal ions such as Cd^{2+}, Pb^{2+}, Hg^{2+} and Zn^{2+}. In addition to metal coordination, these receptors retain the ability to bind anionic species such as chloride. Upon metal complexation, substantial changes in the UV-visible absorption spectra were observed and structural insights from X-ray crystallography and spectroscopic data suggest the formation of 2 : 1 (ligand : metal) complexes, which appear to be the predominant binding mode under the conditions employed. Transport studies using the FluoZin-3 liposome assay revealed that thiosquaramides **3–7** function as highly effective Zn^{2+} ionophores in stark contrast to their oxosquaramide counterparts which showed no measurable ion transport under the same conditions. Furthermore, the chloride transport activity of thiosquaramides was significantly influenced in the presence of Zn^{2+}, consistent with a co-transport mechanism.

Importantly, evaluation of the antimicrobial activity of these compounds against *Staphylococcus aureus* revealed that zinc addition leads to a pronounced enhancement in bacterial growth inhibition. For several members of the series, this effect manifests as a clear Zn^{2+}-dependent "switch-on" of antimicrobial activity. These findings suggest that efficient co-transport perturbs ionic homeostasis within the bacterial cell, contributing to the observed antimicrobial effect—an interpretation further supported by preliminary confocal microscopy data. Taken together, these results introduce thiosquaramides as a promising new class of ionophoric scaffolds, capable of mediating both cation and anion transport and offering tunable biological activity. These results lay the groundwork for further exploration into the structural optimisation of thiosquaramide-based systems and their broader application in supramolecular medicinal chemistry, particularly in the development of novel antimicrobial agents with dual-function transport capabilities.

Author contributions

R. B. P. E., J. F., S. R. and K. K. conceived and designed the study. X.L., L. E. B., C. S. H., T. K., R. B. P. E. and K. K. wrote the manuscript. R. B. P. E. and K. K. supervised the study. X. L. synthesised the compounds under study, carried out spectroscopic titrations and transport studies. L. E. B. performed all biological experiments. C. S. H. carried out X-ray crystallographic analysis. T. K. carried out computational analysis. All authors discussed the results and commented on the manuscript.

Conflicts of interest

There are no conflicts to declare.

Data availability

All relevant experimental details, characterisation data, computational data and binding titration data are presented in the main text and supplementary information (SI). Supplementary information: synthesis, characterisation, NMR titrations and UV-vis titrations, and crystallographic data. See DOI: **https://doi.org/10.1039/d5ob01166c**.

CCDC 2324085–2324087 contain the supplementary crystallographic data for this paper.[56a–c]

Acknowledgements

L. E. B. thanks the Irish Research Council (IRC) for a Government of Ireland Postgraduate Scholarship (GOIPG/2020/78). X. L. acknowledges SSPC, the Research Ireland Centre for Pharmaceuticals and Maynooth University for funding. R. B. P. E. and K. K. acknowledge funding from Science Foundation Ireland (SFI) (grant number: 12/RC/2275/P2), which is co-funded under the European Regional Development Fund. SFI is also acknowledged for funding of the NMR facility (12/RI/2346/SOF) through the Research Infrastructure Programme.

References

1 A. A. Abogunrin, S. A. Healy, O. Fenelon and R. B. P. Elmes, *Chemistry*, 2022, **4**, 1288–1299.
2 L. Qin, A. Hartley, P. Turner, R. B. P. Elmes and K. A. Jolliffe, *Chem. Sci.*, 2016, **7**, 4563–4572.
3 G. M. Chinigo, E. L. McInturff, S. W. Bagley, R. W. Barnhart, D. C. Blakemore, L. Han, T. Lee, J. Magano, J. C. McWilliams, S. Monfette, J. J. Mousseau, S. Pan, D. Pedro, H. H. Perfect, J. W. Raggon, P. R. Rose, J. Sagal, J. I. Trujillo, J. Van Haitsma, M. G. Vetelino and X. H. Yang, *Org. Process Res. Dev.*, 2024, **28**, 2247–2259.
4 L. A. Marchetti, L. K. Kumawat, N. Mao, J. C. Stephens and R. B. P. Elmes, *Chem*, 2019, **5**, 1398–1485.
5 J. P. Malerich, K. Hagihara and V. H. Rawal, *J. Am. Chem. Soc.*, 2008, **130**, 14416–14417.
6 K. A. Agnew-Francis and C. M. Williams, *Chem. Rev.*, 2020, **120**, 11616–11650.
7 A. Singh, A. Torres-Huerta, T. Vanderlinden, N. Renier, L. Martínez-Crespo, N. Tumanov, J. Wouters, K. Bartik, I. Jabin and H. Valkenier, *Chem. Commun.*, 2022, **58**, 6255–6258.

8 J. H. Yang and S. K. Kim, *Chem. Commun.*, 2023, **59**, 9988–9991.
9 M. Vega, L. Martínez-Crespo, M. Barceló-Oliver, C. Rotger and A. Costa, *Org. Lett.*, 2023, **25**, 3423–3428.
10 J. D. E. Lane and K. A. Jolliffe, *Org. Biomol. Chem.*, 2023, **21**, 3226–3234.
11 G. Picci, M. Kubicki, A. Garau, V. Lippolis, R. Mocci, A. Porcheddu, R. Quesada, P. C. Ricci, M. A. Scorciapino and C. Caltagirone, *Chem. Commun.*, 2020, **56**, 11066–11069.
12 M. A. Scorciapino, G. Picci, R. Quesada, V. Lippolis and C. Caltagirone, *Membranes*, 2022, **12**, 292.
13 D. Jagleniec, M. Wilczek and J. Romański, *Molecules*, 2021, **26**, 2751.
14 M. Zaleskaya-Hernik, E. Megiel and J. Romański, *J. Mol. Liq.*, 2022, **361**, 119600.
15 S. Mommer and S. J. Wezenberg, *ACS Appl. Mater. Interfaces*, 2022, **14**, 43711–43718.
16 G. Picci, J. Milia, M. C. Aragoni, M. Arca, S. J. Coles, A. Garau, V. Lippolis, R. Montis, J. B. Orton and C. Caltagirone, *Molecules*, 2021, **26**, 1301.
17 M. Zaleskaya, D. Jagleniec, M. Karbarz, Ł. Dobrzycki and J. Romański, *Inorg. Chem. Front.*, 2020, **7**, 972–983.
18 J. D. E. Lane, G. Shiels, P. Ramamurthi, M. Müllner and K. A. Jolliffe, *Macromol. Rapid Commun.*, 2025, **46**, 2300406.
19 G. Picci, I. Carreira-Barral, D. Alonso-Carrillo, C. Busonera, J. Milia, R. Quesada and C. Caltagirone, *Org. Biomol. Chem.*, 2022, **20**, 7981–7986.
20 M. Zaleskaya, D. Jagleniec and J. Romański, *Dalton Trans.*, 2021, **50**, 3904–3915.
21 M. Yu, Y. Hou, M. Cheng, Y. Liu, C. Ling, D. Zhai, H. Zhao, Y. Li, Y. Chen, X. Xue, X. Ma, M. Jia, B. Wang, P. Wang and M. Li, *Antibiotics*, 2022, **11**, 1497.
22 M. Quintana, J. V. Alegre-Requena, E. Marqués-López, R. P. Herrera and G. Triola, *MedChemComm*, 2016, **7**, 550–561.
23 N. Busschaert, R. B. P. Elmes, D. D. Czech, X. Wu, I. L. Kirby, E. M. Peck, K. D. Hendzel, S. K. Shaw, B. Chan, B. D. Smith, K. A. Jolliffe and P. A. Gale, *Chem. Sci.*, 2014, **5**, 3617–3626.
24 M. Berney, W. Doherty, W. T. Jauslin, M. T. Manoj, E.-M. Dürr and J. F. McGouran, *Bioorg. Med. Chem.*, 2021, **46**, 116369.
25 R. B. P. Elmes, N. Busschaert, D. D. Czech, P. A. Gale and K. A. Jolliffe, *Chem. Commun.*, 2015, **51**, 10107–10110.
26 A. Arun, A. Docker, H. M. Tay and P. D. Beer, *Chem. – Eur. J.*, 2023, **29**, e202301446.
27 L. A. Marchetti, T. Krämer and R. B. P. Elmes, *Org. Biomol. Chem.*, 2022, **20**, 7056–7066.
28 A. Grundzi, S. A. Healy, O. Fenelon and R. B. P. Elmes, *Results Chem.*, 2022, **4**, 100652.
29 L. K. Kumawat, A. A. Abogunrin, M. Kickham, J. Pardeshi, O. Fenelon, M. Schroeder and R. B. P. Elmes, *Front. Chem.*, 2019, **7**, 354.
30 L. E. Brennan, X. Luo, F. A. Mohammed, K. Kavanagh and R. B. P. Elmes, *Chem. Sci.*, 2025, **16**, 4075–4084.
31 L. E. Brennan, L. K. Kumawat, M. E. Piatek, A. J. Kinross, D. A. McNaughton, L. Marchetti, C. Geraghty, C. Wynne, H. Tong, O. N. Kavanagh, F. O'Sullivan, C. S. Hawes, P. A. Gale, K. Kavanagh and R. B. P. Elmes, *Chem*, 2023, **9**, 3138–3158.
32 R. P. Daniele and S. K. Holian, *Proc. Natl. Acad. Sci. U. S. A.*, 1976, **73**, 3599–3602.
33 D. Łowicki and A. Huczyński, *BioMed Res. Int.*, 2013, **2013**, 742149.
34 M. Mitani, T. Yamanishi and Y. Miyazaki, *Biochem. Biophys. Res. Commun.*, 1975, **66**, 1231–1236.
35 S. Scavo and V. Oliveri, *J. Inorg. Biochem.*, 2022, **228**, 111691.
36 L. Bohlmann, D. M. P. De Oliveira, I. M. El-Deeb, E. B. Brazel, N. Harbison-Price, C. Y. Ong, T. Rivera-Hernandez, S. A. Ferguson, A. J. Cork, M.-D. Phan, A. T. Soderholm, M. R. Davies, G. R. Nimmo, G. Dougan, M. A. Schembri, G. M. Cook, A. G. McEwan, M. von Itzstein, C. A. McDevitt and M. J. Walker, *mBio*, 2018, **9**, e02391–e02318.
37 N. Harbison-Price, S. A. Ferguson, A. Heikal, G. Taiaroa, K. Hards, Y. Nakatani, D. Rennison, M. A. Brimble, I. M. El-Deeb, L. Bohlmann, C. A. McDevitt, M. von Itzstein, M. J. Walker and G. M. Cook, *mSphere*, 2020, **5**, DOI: **10.1128/msphere.00157-20**.
38 N. Renier, O. Reinaud, I. Jabin and H. Valkenier, *Chem. Commun.*, 2020, **56**, 8206–8209.
39 A. Rostami, A. Colin, X. Y. Li, M. G. Chudzinski, A. J. Lough and M. S. Taylor, *J. Org. Chem.*, 2010, **75**, 3983–3992.
40 J. Bergman, B. Pettersson, V. Hasimbegovic and P. H. Svensson, *J. Org. Chem.*, 2011, **76**, 1546–1553.
41 M. Rombola and V. H. Rawal, *Org. Lett.*, 2018, **20**, 514–517.
42 R. Chakrabarty, S. J. Bora and B. K. Das, *Inorg. Chem.*, 2007, **46**, 9450–9462.
43 K. B. Wiberg and Y. Wang, *ARKIVOC*, 2010, **2011**, 45–56.
44 Y.-L. Wu and A. I. Wright, *Phys. Chem. Chem. Phys.*, 2023, **25**, 1342–1348.
45 V. Amendola, G. Bergamaschi, M. Boiocchi, L. Fabbrizzi and M. Milani, *Chem. – Eur. J.*, 2010, **16**, 4368–4380.
46 P. Thordarson, *Chem. Soc. Rev.*, 2011, **40**, 1305–1323.
47 D. B. Hibbert and P. Thordarson, *Chem. Commun.*, 2016, **52**, 12792–12805.
48 N. Busschaert, I. L. Kirby, S. Young, S. J. Coles, P. N. Horton, M. E. Light and P. A. Gale, *Angew. Chem., Int. Ed.*, 2012, **51**, 4426–4430.
49 L. E. Brennan and R. B. P. Elmes, *Trends Chem.*, 2025, **7**, 354–357.
50 O. N. Kavanagh, S. Bhattacharya, L. Marchetti, R. Elmes, F. O'Sullivan, J. P. Farragher, S. Robinson, D. Thompson and G. M. Walker, *Pharmaceutics*, 2022, **14**, 899.
51 A. Hecel, M. Ostrowska, K. Stokowa-Sołtys, J. Wątły, D. Dudek, A. Miller, S. Potocki, A. Matera-Witkiewicz, A. Dominguez-Martin, H. Kozłowski and M. Rowińska-Żyrek, *Pharmaceuticals*, 2020, **13**, 228.
52 V. Frazzini, A. Granzotto, M. Bomba, N. Massetti, V. Castelli, M. d'Aurora, M. Punzi, M. Iorio, A. Mosca,

S. Delli Pizzi, V. Gatta, A. Cimini and S. L. Sensi, *Sci. Rep.*, 2018, **8**, 9768.

53 Role of Zinc and Zinc Ionophores in Brain Health and Depression Especially during the COVID-19 Pandemic| IntechOpen, **https://www.intechopen.com/chapters/80582**, (accessed August 14, 2023).

54 S. Yoshino, A. Hara, H. Sakakibara, K. Kawabata, A. Tokumura, A. Ishisaka, Y. Kawai and J. Terao, *Nutrition*, 2011, **27**, 847–852.

55 E. E. Hickey, S. W. Page and D. J. Trott, *J. Vet. Pharmacol. Ther.*, 2020, **43**, 499–507.

56 (*a*) CCDC 2324085: Experimental Crystal Structure Determination, 2025, DOI: **10.5517/ccdc.csd.cc2j0dhg**; (*b*) CCDC 2324086: Experimental Crystal Structure Determination, 2025, DOI: **10.5517/ccdc.csd.cc2j0djh**; (*c*) CCDC 2324087: Experimental Crystal Structure Determination, 2025, DOI: **10.5517/ccdc.csd.cc2j0dkj**.